ACS Photonics

Letter

Cite This: ACS Photonics 2019, 6, 620−627

pubs.acs.org/journal/apchd5

Orbital Angular Momentum and Energy Loss Characterization of Plasmonic Excitations in Metallic Nanostructures in TEM

Matteo Zanfrognini,[†,‡] Enzo Rotunno,[*,‡] Stefano Frabboni,[†,‡] Alicia Sit,[§] Ebrahim Karimi,[§] Ulrich Hohenester,[∥] and Vincenzo Grillo[‡]

[†]Dipartimento FIM, Università di Modena e Reggio Emilia, Via G. Campi 213/a, I-41125, Modena, Italy

[‡]CNR-NANO Via G. Campi 213/a, I-41125, Modena, Italy

[§]Department of Physics, University of Ottawa, 150 Louis Pasteur, Ottawa, Ontario K1N 6N5, Canada

[∥]Institute of Physics, Karl-Franzens-Universitat Graz, Universitatsplatz 5, 8010 Graz, Austria

Supporting Information

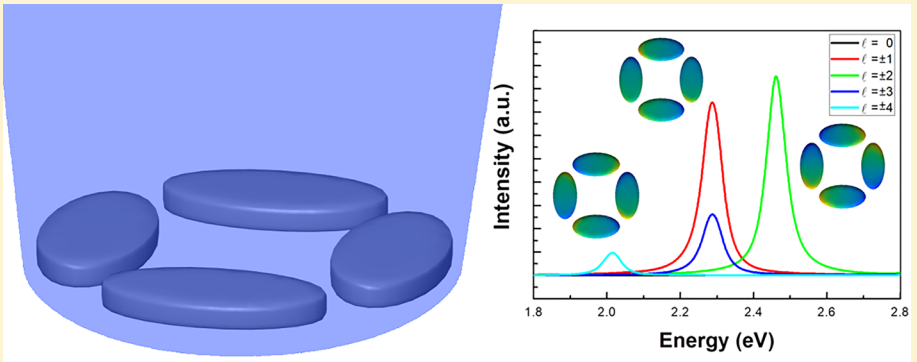

ABSTRACT: Recently, a new device to measure the orbital angular momentum (OAM) electronic spectrum after elastic/inelastic scattering in a transmission electron microscope has been introduced. We modified the theoretical framework needed to describe conventional low-loss electron energy loss spectroscopy (EELS) experiments in transmission electron microscopes (TEM) to study surface plasmons in metallic nanostructures, to allow for an OAM post selection and devise new experiments for the analysis of these excitations in nanostructures. We found that unprecedented information on the symmetries and on the chirality of the plasmonic modes can be retrieved even with limited OAM and energy resolutions.

KEYWORDS: *plasmonics, electron energy loss spectroscopy, electron orbital angular momentum, transmission electron microscopy*

Localized surface plasmon resonances are confined collective excitations of the conduction electrons in a metallic nanostructure, whose excitation energies depend both on the material and on the geometrical shape of the nanoparticle itself. In the past few years, the properties of these peculiar resonances have become a topic of great interest in the context of physics, chemistry, and material science. They have potential applications in a wide range of fields, from medicine[1] to SERS spectroscopy,[2] and from optoelectronics to photovoltaics.[3]

The primary technique for characterizing plasmon resonances is through exciting them with light in absorption and scattering experiments. The main limitations of this approach are (1) only the modes with a nonvanishing electric dipole (bright modes) can be excited and (2) the local fields associated with these excitations are not spatially mapped with enough resolution. A more flexible approach to their analysis is represented by electron energy loss spectroscopy (EELS) performed in a transmission electron microscope (TEM). EELS can spatially map, with subnanometer resolution, the fields associated with both bright and dark plasmonic resonances of a given metallic nanostructure.[4−6]

In a typical EELS experiment, an electron probe with subnanometer transverse size is scanned on different points on the sample surface R, and the loss function $\Gamma(E, R)$ is evaluated at the excitation energy E of a certain plasmonic resonance. As clearly shown by Boudarham and Kociak,[7] this quantity turns out to be proportional to the square modulus of the electric field associated with this resonance, evaluated at point R and projected along the TEM optical axis. It can be seen immediately that this approach prevents the experimental measurement of the local phase (i.e., of the sign) of the fields characterizing these excitations; simultaneously, modes with energy separations smaller than the energetic resolution of the experimental apparatus are extremely difficult to resolve.

A first attempt to have direct access to the phase of the excitations has been produced by Guzzinati and co-workers,[8]

Received: January 24, 2019
Published: February 22, 2019

DOI: 10.1021/acsphotonics.9b00131
ACS Photonics 2019, 6, 620−627

who adopted a structured beam and collected only on-axis inelastically scattered electrons; in this way, only the energy loss due to the mode with spatial symmetry matching that of the incoming wave can be detected. Possible limitations to this innovative approach could be (1) the requirement of using different structured beams (and, therefore, different measurements) to access the whole plasmonic spectrum of a nanostructure; (2) the necessity of preliminary knowledge of the spatial symmetries of the plasmon resonances to be probed (in order to choose an appropriate incoming electron wave); and (3) the fact that collecting only the inelastically scattered electrons along the TEM axis means decreasing the signal-to-noise ratio in the probed quantities.[9]

It has been recently demonstrated experimentally the possibility of measuring the orbital angular momentum spectrum of a light[10] or an electron beam:[11,12] this type of measurement is possible by inserting two phase elements (orbital angular momentum (OAM) sorters) in the TEM column, performing the coordinate transformation from position to angular basis representation of the wave function.[13] Here, starting from the theoretical approach proposed in ref 8, we demonstrate the possibility of gaining information about the symmetries of the plasmonic fields by measuring not only the energy spectrum of the inelastically scattered electrons but also their OAM spectrum, without using multiple structured beams as initial probes: so, differently from previous approaches we concentrate on measuring the final OAM state, keeping the initial state constant. By setting up the electron microscope similarly to what is explained in ref 11 (see Supporting Information Figure S1 for more details about the electron optics configuration) it will be possible to disperse the OAM and energy loss spectra of the transmitted electrons in orthogonal directions, thus having access to the so-called OAM-resolved loss functions $\Gamma_l(E)$

In the following, we will simulate the expected experimental results in a number of paradigmatic cases, while considering the effects of the finite resolutions in both energy and OAM due to a nonideal experimental setup. We demonstrate how such a double dispersed experiment could give access to novel information about plasmonic fields, with respect to conventional EELS measurements.

We provide now a brief description about how it is possible to simulate OAM-resolved electron energy loss spectra. We start by describing the interaction between a probe electron in $\vec{r}$ and the charge density $\rho(\vec{r}\,')$ of the nanostructure through the following interaction Hamiltonian:

$$\hat{H}' = -\int e\frac{\rho(\vec{r}\,')}{|\vec{r}-\vec{r}\,'|}\mathrm{d}^3r' \tag{1}$$

where the integration is performed over the nanoparticle's (NP) volume, and e is the charge of the electron. For a weak interaction, the transition probability (Γ) from an initial electronic state Ψ_i (with energy E_0) to a final state Ψ_f^l, with an OAM value of $l\hbar$ is given using Fermi's golden rule as

$$\Gamma \propto \sum_{f,n}\left|\int\int \mathrm{d}\vec{r}\ \mathrm{d}\vec{r}\,'\frac{\Psi_f^*(\vec{r})\,\Psi_i(\vec{r}\,')}{|\vec{r}-\vec{r}\,'|}\langle n|\rho(\vec{r}\,')|0\rangle\right|^2 \times \delta(E_f - E_0 + \varepsilon_n - \varepsilon_0) \tag{2}$$

Here, the OAM is defined along the probe electron's direction of propagation, i.e., the TEM optical axis (taken to be the z-axis), and $|0\rangle$ and $|n\rangle$ are respectively the ground state of the nanoparticle (with energy ε_0) and its nth excited state. Exploiting the definition of electronic susceptibility $\chi(\vec{r}, \vec{r}\,', E)$ given in ref 14 and references therein, and considering only transitions for the probing electron to states with energy $E_f = E_0 - E$, it is possible to write

$$\Gamma_l(E) \propto \sum_f \int\int \mathrm{d}\vec{r}\ \mathrm{d}\vec{r}\,'\Psi_f^l(\vec{r})\,\Psi^*{}_i(\vec{r})\,\mathrm{Im}(-W(\vec{r}, \vec{r}\,', E)) \times\Psi_f^{l*}(\vec{r}\,')\,\Psi_i(\vec{r}\,')\,\delta(E_f + E - E_0) \tag{3}$$

with $W(\vec{r}, \vec{r}\,', E)$ being the screened interaction between an electron in $\vec{r}$ and one in $\vec{r}\,'$. Following the approach shown in ref 7, we can write such a function as

$$W(\vec{r}, \vec{r}\,', E) = \sum_m g_m(E)\,\phi_m(\vec{r})\,\phi_m(\vec{r}\,')^* \tag{4}$$

where $\phi_m(\vec{r})$ is the potential associated with the mth surface plasmon resonance of the metallic nanostructure, and $g_m(E)$ is the so-called spectral function.

In the paraxial approximation, we take

$$\Psi_{in}(x, y, z; \overrightarrow{K_{in}}) = e^{iK_{in}{}^z z}\psi_{in}(x, y) \tag{5.1}$$

$$\Psi_f^l(x, y, z; \overrightarrow{K_f}) = e^{iK_f{}^z z}\psi_f^l(x, y) \tag{5.2}$$

where $\psi_{in}(x,y)$ ($\psi_f^l(x, y)$) denotes the initial (final) electronic wave function in a plane perpendicular to the optical axis, while $\overrightarrow{K_{in}}$ and $\overrightarrow{K_f}$ are the electron wavevectors before and after the scattering process. This approach is correct every time $K_{in}{}^z$ and K_f^z are much larger than the projection of the wavevector perpendicular to the optical axis.

By substitution of eqs 4, 5.1, and 5.2 in eq 3, using nonrecoil approximation,[14] summing over all the possible K_f^z (exploiting the delta function in eq 3), and performing the integration along z, we finally obtain the desired OAM-resolved loss function:

$$\Gamma_l(E) \propto \sum_f\sum_m \mathrm{Im}(-g_m(E)) \times\left|\iint \mathrm{d}x\ \mathrm{d}y\ \psi_f^{\,l}(x, y)\,\phi_m(x, y, q)\,\psi_i(x, y)^*\right|^2 \tag{6}$$

while $\varphi_m(x, y, q)$ is the Fourier transform along z of the potential $\phi_m(\vec{r})$.[15]

In the following calculations, we will assume $\psi_i(x, y)$ to be a Gaussian beam whose waist is comparable with the size of the plasmonic nanoparticles, while we will write the final electronic states $\psi_f^l(x, y)$ as[16,17]

$$\psi_f(x, y) = J_{|l|}(K_f r)e^{il\varphi} \tag{7}$$

in which $J_{|l|}(K_f r)$ is a Bessel function of the first kind of order e, K_f is the transverse wavevector (i.e., the projection of the electron wavevector $\overrightarrow{K_f}$ on the xy plane, perpendicular to the optical axis), and l is the winding number. In this way, the sum over the index f appearing in eq 6 is now performed over an ensemble of such final states characterized by a fixed e and with transverse wavevector K_f in the interval $[0, K_{Max}]$, where K_{Max} depends on the collection angle α of the detector as $\alpha = K_{Max}\lambda$,

DOI: 10.1021/acsphotonics.9b00131
ACS Photonics 2019, 6, 620−627

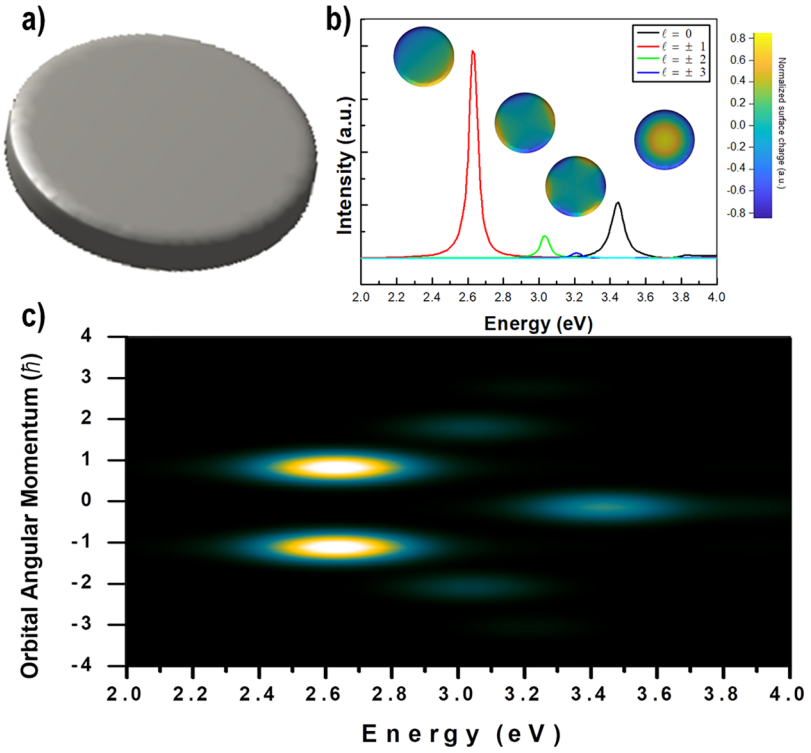

Figure 1. (a) Tilted view of the Ag nanodisk. (b) Simulated OAM-resolved EEL spectra for different OAM values (see legend). The surface charge distribution of each plasmonic mode is reported as an inset, where positive (negative) charge corresponds to blue (yellow) tone. (c) 2D representation of the EEL spectra convoluted with a Gaussian function simulating the limited instrumental resolution (ΔE = 0.3 eV and $\Delta l = 0.5\hbar$).

with λ corresponding to the electron's de Broglie wavelength. In the following calculations, we have kept K_{Max} fixed to 0.4 nm^{-1} (semicollection angles of about 1 mrad,; see Supporting Information Figure S2), while the electron energy E_0 has been taken equal to 300 keV. Such an approach permits also to eventually include structured incoming electron beams, such as, for example, vortices and two-lobed profiles as proposed respectively by refs 18, 19, and 8. Our choice of using Gaussian beams with quite large beam waists is only associated with the possibility of exciting all the different plasmonic resonances of the nanostructure at the same time. In any case, our results are not dependent on the choice of using an effectively Gaussian electron beam profile; a plane-wave-like illumination gives qualitatively the same results, changing only the relative intensities of the peaks related to different modes). The spectral function $g_m(E)$ depends on both the geometry and the dielectric properties of the considered metallic nanostructure, and its imaginary part (with a minus sign) is maximized at the mth surface plasmon resonance (SPR) energy. The analytical form of the imaginary part of this function is analogous to the one provided in ref 7 by Boudarham and Kociak considering the metallic nanostructure embedded in a homogeneous medium with constant dielectric function and neglecting the contribution to the electron energy loss due to bulk excitations. Finally, $\phi_m(x, y, q)$ is the Fourier transform, along z, of the electric potential associated with the mth plasmonic mode; such a quantity does not depend on the dielectric properties of the material but only on the geometry of the considered sample.

Within this approach, the surface plasmon oscillations are treated classically, i.e., by computing the plasmon response function solving Maxwell's equations in the nonretarded approximation through the boundary element method,[14,15] implemented in the MNPBEM toolbox.[20] The electron dynamics, however, are studied quantum mechanically using Fermi's golden rule, as outlined above. In the adopted theory, we neglect the contribution to the electron energy loss due to bulk plasmon excitations of the metal, as their energies are expected to be larger than those of the localized surface plasmons of interest. We also suppose the nanostructure to be embedded in a vacuum, neglecting in this way the effect of the substrate on which the structures are located. As reported in ref 21, the effect of the substrate is both to red shift the SPR resonances and to increase the line widths of the plasmonic features, but the symmetry properties of the excitations, in which we are interested, are expected to be left unchanged by the substrate itself. As a final remark, we also point out that neglecting retardation effects should mainly give a blue-shift of the excitation energies,[14] while leaving unchanged the symmetries of the modes that are the target of the proposed experiments. In any case, although in this work we have employed for simplicity the quasi-static approximation throughout, future work should also address the case of the full Maxwell's equations where a modal decomposition into resonance modes could be performed, in analogy to refs 22 and 23.

The first example of OAM analysis of the inelastically scattered electrons by surface plasmons that we consider is the case of a nanostructure with cylindrical symmetry. We explore the didactic case of a nanodisk, but the following description can be extended to the case of any axially symmetric system such as toroidal or spherical particles.

Because of the peculiar symmetry of this nanostructure, we expect the surface charge distributions associated with the

DOI: 10.1021/acsphotonics.9b00131
ACS Photonics 2019, 6, 620−627

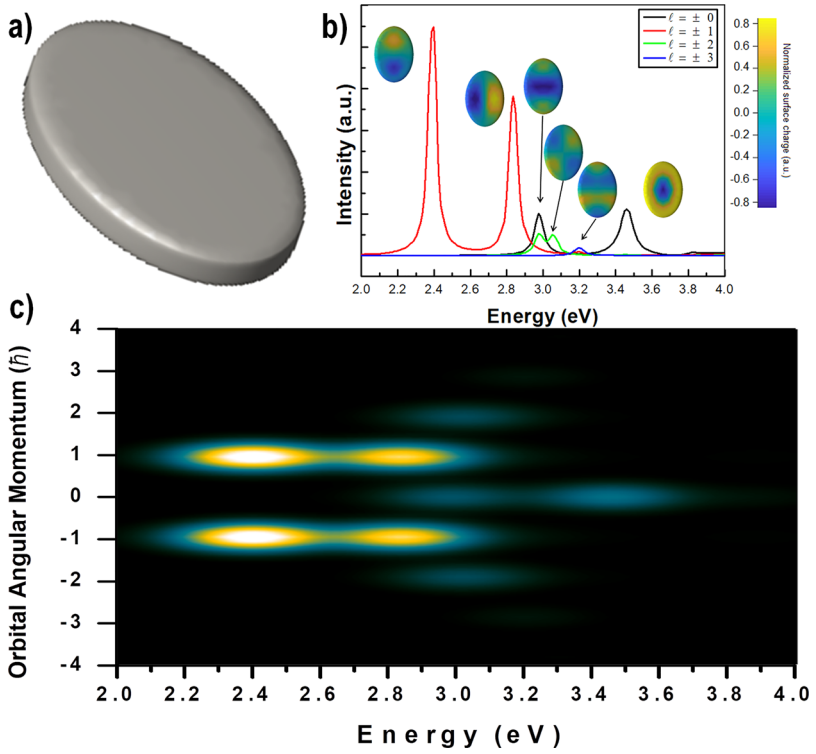

Figure 2. (a) Tilted view of the Ag elliptical nanodisk. (b) Simulated OAM-resolved EEL spectra for different OAM values (see legend). The surface charge distribution of each plasmonic mode is reported as insets. (c) 2D representation of the EEL spectra convoluted with a Gaussian function simulating the limited instrumental resolution (ΔE = 0.3 eV and $\Delta l = 0.5\hbar$): notice a common strong intensity at about 3.0 eV for both $l = \pm 2$ and $l = 0$, pointing out the hybridization of the quadrupolar and the breathing modes of the nanodisk.

different plasmonic modes to be characterized by an azimuthal dependence of the type $\cos(m\delta)$ or $\sin(m\delta)$, where m is a positive or null integer number. The same azimuthal behavior is expected to be inherited by the associated electric eigenpotential $\phi_m(x, y, q) = \phi_m(r)\frac{e^{im\varphi} \pm e^{-im\varphi}}{2}$, where $\varphi_m(r)$ describes the radial behavior of the potential itself[24] (see Supporting Information for a further clarification of this point, in particular Figure S4). Taking as incident state $\psi_i(r)$ a nonstructured beam (e.g., a Gaussian beam with transverse dimensions at least equal to the nanoparticle diameter or a plane wave), the transition probability to a final state characterized by an OAM value of l (i.e., $\Gamma_l(E)$), expressed in cylindrical coordinates, becomes

$$\Gamma_l(E) \propto \sum_{K_f}\sum_{m}\left|\int dr \int_0^{2\pi} rJ_{|l|}(K_f r)e^{il\varphi}\phi_m(r)(e^{im\varphi} \pm e^{-im\varphi})\psi_i(r)^* \, d\varphi\right|^2 \quad (8)$$

which gives us the selection rule

$$\int_0^{2\pi} e^{i\varphi(l\pm m)}d\varphi \neq 0 \leftrightarrow l = \mp m \quad (9)$$

Summarizing, each $\Gamma_l(E)$ is a function with peaks only at the excitation energies of the modes characterized by $m = l$; therefore, in an OAM-resolved EELS experiment, one is able to distinguish the plasmonic resonances both according to their energy and their azimuthal symmetries with only a single measurement.

As an example, we performed numerical calculations for a silver nanodisk (silver dielectric function has been taken from Johnson[25]), with a height of 10 nm and a diameter of 70 nm (Figure 1a). The sample is illuminated by a Gaussian beam with a beam waist equal to 35 nm centered in the middle of the disk. We consider the behavior of the loss function in the interval of energies [2; 4] eV, where the first plasmonic modes locate in energy. The simulated OAM-resolved EEL spectra, for different values of l, are reported in Figure 1b. As expected, for each OAM value, we have a peak at the energy of the plasmonic mode with the corresponding azimuthal symmetry. Therefore, the intense maximum observed in the spectrum obtained for $l = \pm 1$ corresponds to the dipolar edge mode (depicted in the inset), while the peaks found for $\Gamma_{\pm 2}$ and $\Gamma_{\pm 3}$ are respectively due to the quadrupolar and the hexapolar edge resonances of the nanodisk. As a last remark, the maximum observed for $l = 0$ is related to the breathing mode of the nanodisk,[26] which is characterized by an eigenpotential not dependent on the variable φ.

Despite the results of the performed simulations fitting our precedent reasoning, from the experimental point of view, resolving the inelastically scattered electrons both in energy and in OAM is a difficult task. In particular, the limited instrumental resolution of the analyzing system must be taken into account in order to obtain results that can be, in some way, compared with those found experimentally. In order to show the results closer to a realistic experiment, we have convolved the numerically obtained loss functions $\Gamma_l(E)$ with a Gaussian function taking into account the broadening introduced by the experimental apparatus (see Supporting Information Figure S3). The result is reported in Figure 1c, where the values ΔE = 0.3 eV and $\Delta l = 0.5\hbar$ are used for the

DOI: 10.1021/acsphotonics.9b00131
ACS Photonics 2019, 6, 620−627

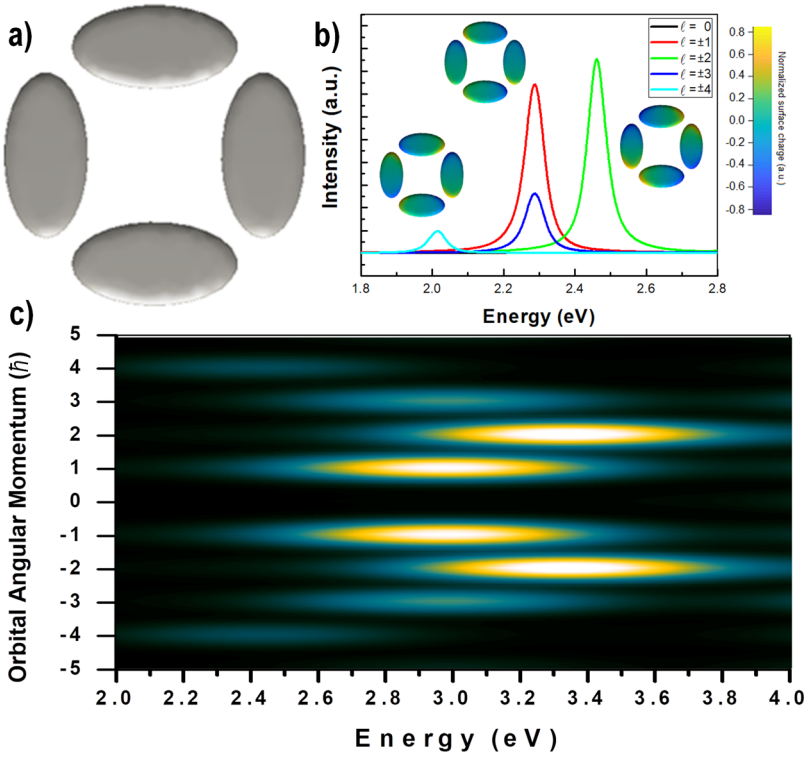

Figure 3. (a) Top view of the plasmonic molecule composed of four identical Ag elliptical nanodisks. (b) Simulated OAM-resolved EEL spectra for different OAM values (see legend). The surface charge distribution of each plasmonic mode is reported as insets. (c) 2D representation of the EEL spectra convoluted with a Gaussian function simulating the limited instrumental resolution (ΔE = 0.3 eV and $\Delta l = 0.5\hbar$).

energy and OAM resolution, respectively; these values are consistent with the resolution of modern state-of-the-art monochromated electron microscopes.[14,24] The simulation shows that, despite the experimental broadening, every loss function $\Gamma_l(E)$ is still distinctly peaked at the corresponding energies. This is an effect of experiments that are doubly dispersed in energy and OAM so that energy resolution by itself is not the main limiting factor. We further noticed that, if the resolution is decreased to ΔE = 1 eV as for a nonmonochromatized Schottky field emission gun (FEG), thanks to the double OAM and energy loss dispersion, we are still able to capture the difference between the dipole and breathing modes.

As stated above, for systems with cylindrical (or more generally axial) symmetry, the surface plasmon modes are characterized by a well-defined azimuthal behavior. If the symmetry is slightly broken, for example considering the structure shown in Figure 2a, the surface charge no longer follows the simple azimuthal distribution described above. In any case, it is reasonable to expect that, by destroying the cylindrical symmetry, the resulting modes can still be written as a superposition of the nanodisk modes.[27] We can thus expect that a given plasmonic resonance of the morphed structure can have a surface charge distribution (and so an eigenpotential) given by the sum of functions with a φ dependence of the type $\cos(m\varphi)$ or $\sin(m\varphi)$, with different values of m for the same plasmonic mode (see Supporting Information Figure S5 and Figure S6 for a complete decomposition of some of the resonances of the morphed structure). Taking into account what was explained before, we then expect to observe peaks at the same energy for loss functions computed for different l. More clearly, if at the excitation energy E_α of the mode α of the deformed disk we have a maximum for both $\Gamma_{\pm m_1}(E_\alpha)$ and $\Gamma_{\pm m_2}(E_\alpha)$, it means that such a resonance can be understood as given by the hybridization of the modes with azimuthal numbers m_1 and m_2 of the nanodisk:[27] such information cannot be gained using conventional EELS techniques.

We performed simulations for the structure shown in Figure 2a: a nanoellipse that has been obtained distorting the nanodisk in Figure 1a according to the approach described in the Supporting Information (the major axis is equal to 84 nm, while the minor one is 60 nm). We assume an incoming beam analogous to the one adopted for the nanodisk.

Looking at the OAM-EEL-resolved spectra reported in Figure 2b, we immediately notice that the two degenerate dipolar edge modes of the nanodisk split in energy and give very intense peaks for $l = \pm 1$. At the same time, it is simple to observe that the functions $\Gamma_{\pm 2}$ and Γ_0 have a common peak at an energy of 2.975 eV; however, $\Gamma_{\pm 2}$ has a maximum at 3.05 eV not observable in the trend of Γ_0. In good agreement with the observations reported in ref 27, this effect can be justified by assuming that the two degenerate quadrupolar edge modes of the nanodisk separate in energy, and the lower energy one mixes with the breathing mode: this common peak for $\Gamma_{\pm 2}$ and Γ_0 at the same energy can be considered as an experimental demonstration of this mode hybridization.

In Figure 2c, we present the expected results of a real life experiment, performing the same convolution procedure outlined in the case of the nanodisk. Even if the two close peaks for $\Gamma_{\pm 2}$ cannot be resolved as their separation is smaller than the assumed broadening in energy, it is immediately noticed that both the loss functions computed for $l = \pm 2$ and $l = 0$ have strong intensities at about 3.0 eV, signaling the

DOI: 10.1021/acsphotonics.9b00131
ACS Photonics 2019, 6, 620−627

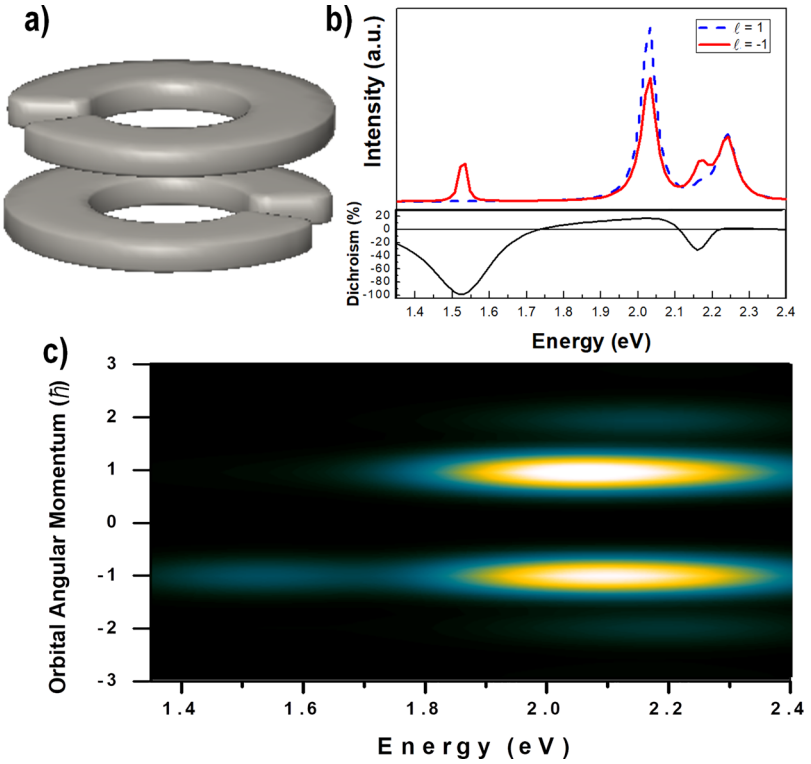

Figure 4. (a) Tilted view of the chiral plasmonic structure. (b) Simulated OAM-resolved EEL spectra for the $l = +1$ (blue dashed line) and $l = -1$ (red line) components: notice the presence of a peak only for $l = -1$ at 1.53 eV, which is responsible for a giant electron dichroism effect. (c) 2D representation of the EEL spectra convoluted with a Gaussian function simulating the limited instrumental resolution ($\Delta E = 0.3eV$ and $\Delta l = 0.5\hbar$). It is immediately observed, despite the experimental broadening, a very pronounced asymmetry between the signals for $l = +1$and $l = -1$.

mode mixing described before, even with a nonideal experimental setup.

OAM-resolved EELS experiments are well suited for studying the azimuthal behavior of plasmon resonances in noncylindrically symmetric nanostructures, such as the nanoellipse, but the discussion can be naturally extended to more complex, and technologically appealing, systems. This is the case of the plasmon resonances of cyclic formations of metal nanoparticles, known as metamolecules or plasmonic oligomers,[28−30] which are characterized by magnetic excitations.[31]

We consider here the case of the system reported in Figure 3a, composed of four identical elliptical nanodisks, each one having a major axis, a minor axis, and a height measuring 120, 60, and 10 nm, respectively. The nanoparticles are disposed along the 160 nm long sides of a square, resulting in a minimum distance between them of 21 nm, and they are illuminated with a Gaussian beam with a large beam waist (300 nm), centered in the middle of the square.

Figure 3b shows the calculated OAM-resolved EEL spectra in the energy range spanning from 1.8 to 2.8 eV, where the first three plasmonic modes, in order of energy, are located. Alongside each loss peak, reported as insets, are the respective surface charge distributions.

The lowest energy plasmon mode (2.02 eV) is characterized by a surface charge distribution (and so a potential) that changes its sign eight times in a complete path around the axis of the structure (see Supporting Information Figure S7 for further discussion). It is therefore reasonable to assume a potential with an in-plane azimuthal trend given by $\cos(4\varphi)$ or $\sin(4\varphi)$, which produces only peaks for $\Gamma_{\pm 4}$ at the energy of this mode. Analogously, the charge distribution associated with the resonance at 2.46 eV changes sign four times, so it is associated with a potential with a $\cos(2\varphi)$ or $\sin(2\varphi)$ azimuthal profile, which rationalizes the maxima only for $\Gamma_{\pm 2}$ at this energy.

More complex is, instead, the case of the plasmon peak at 2.28 eV, as the charge distribution behavior with φ cannot be simply deduced graphically. A complete modal decomposition (see Supporting Information Figure S7) suggests that the potential associated with this mode is characterized by very intense contributions of the type $e^{\pm i\varphi}$ and $e^{\pm i3\varphi}$, which give intense peaks for $\Gamma_{\pm 1}$ and $\Gamma_{\pm 3}$ at the energy of this resonance.

With this example, we point out the capability of deriving information about the symmetries and the signs of the potentials associated with plasmon resonances of unconventional nanostructures.

Such an example also underlines the possibility of exploiting such a technique to resolve plasmon resonances that are nearly degenerate in energy. For example, focusing on the two modes at 2.28 and 2.46 eV, even if their energetic separation is smaller than the broadening in energy of the incoming electron beam, their contributions to the electron losses can be separated, as they provide peaks for different Γ_l. This is clearly noticeable once we look at the simulated experimental spectra shown in Figure 3c, where the peaks associated with these two modes are clearly distinguishable, despite the introduced broadening in both energy and OAM.

As a final application of OAM-resolved EELS, we focus on the study of chiral plasmonic nanostructures. As already pointed out by Asenjo Garcia in ref 32, chiral (i.e., not mirror symmetric) 3D plasmonic nanostructures are expected to

DOI: 10.1021/acsphotonics.9b00131
ACS Photonics 2019, 6, 620−627

produce electron OAM dichroism once illuminated by conventional beams, i.e., differences in intensities between the loss functions $\Gamma_{+l}(E)$ and $\Gamma_{-l}(E)$. In order to quantify the strength of such dichroic effects, we have followed ref 32 in defining the following figure of merit as

$$D_{|l|}(E) = 100\frac{\Gamma_{+l}(E) - \Gamma_{-l}(E)}{\Gamma_{+l}(E) + \Gamma_{-l}(E)} \quad (10)$$

The chiral assemblies of metallic nanoparticles analyzed in ref 32 are expected to provide dichroic signals on the order of 10−15%. In the following, we present simulations performed for a metallic nanostructure which should exhibit giant electron dichroism, i.e., values of $D_{|l|}$((for $|l| = 1$) of the order of 100%, which could greatly simplify the experimental detection of this effect (already attempted in ref 33 for a cluster of nanospheres).

This structure in question, reported in Figure 4a, is made of two identical open silver nanorings, each of them characterized by a height of 10 nm, an external radius of 50 nm, and an internal one of 25 nm; the spacing between the two nanorings is 20 nm and the opening angle has been fixed to 30° in all the calculations. The rings are rotated with respect to one another in order to break the mirror symmetry, as one can observe from the image. This structure may remind one of a cylindrical conductor.[34] Such a structure was described in a recent paper in the context of interaction-induced change of the OAM state. However, this structure is deeply different due to the complete break of the symmetry.

In Figure 4b, we show the energy loss spectra for $l = 1$ and $l = -1$, the functions $\Gamma_{+1}(E)$ and $\Gamma_{-1}(E)$, respectively, calculated for an incident Gaussian beam with a beam waist of 50 nm, centered in the common center of the two rings. The comparison of the spectra immediately shows strong differences, in particular at the energy $E' = 1.53$ eV, where the loss function $\Gamma_{-1}(E)$ is predominant, while the opposite polarity $\Gamma_{+1}(E)$ is almost completely absent, leading to a dichroic signal $D_1(E)$ close to 100%, while a dichroic effect (even if much less pronounced) is also present in the peak at 2.17 eV. Conversely, the peak at $E'' = 2.03$ eV is more intense for the $l = 1$ component even though the difference is only $D_1(E'') = 20\%$ (see Supporting Information Figures S8 and S9 for a complete OAM decomposition of these modes). A realistic experiment, simulated in Figure 4c, is also able to observe the dichroism: by comparing the two spectra for $l = +1$ and $l = -1$, one can readily notice the complete absence of the peak at 1.53 eV in the $l = 1$ spectrum: notice that if this energy could be isolated, we would obtain a plasmon-based generation of an electron vortex as in ref 35 but without the use of light to excite the plasmons. The three peaks at 2.03, 2.17, and 2.24 eV cannot be individually resolved due to the limited resolution of the experimental setup; however, the maximum of the broad intensity distribution is shifted, reflecting the different intensity of the peaks. We recall that here we are not considering any postprocessing of the image that can improve the resolution and in principle retrieve the intensity of the single peaks.

In summary, we have demonstrated that, by combining the evaluation of the energy and OAM spectra of inelastically scattered electrons by a plasmonic nanostructure, it is possible to obtain additional information about the symmetries and also the chirality of the fields associated with these systems, by performing only a single measurement, i.e., without the need of modifying the features of the incoming electron wave. We proposed a possible measure to directly experimentally access the way in which plasmon modes mix together once a metallic nanostructure is distorted. We have also pointed out the possibility to exploit the double dispersion in OAM and energy loss to resolve peaks due to plasmon resonances that are separated in energy by a quantity smaller than the experimental resolution. All this information is not achievable exploiting techniques (e.g., conventional EELS in TEM or photoemission electron microscopy) normally used to map the electric fields of localized surface plasmon resonances of structures with characteristic sizes of few tens of nanometers. Furthermore, the use of the OAM sorter could be also very useful in the approach to the inverse problem of retrieving particle shapes by the explicit plasmon characteristics.

■ ASSOCIATED CONTENT

Supporting Information

The Supporting Information is available free of charge on the ACS Publications website at DOI: 10.1021/acsphotonics.9b00131.

Details about the setup needed to perform the proposed experiments and annotations to the performed simulations and to the interpretation of the presented simulated spectra (PDF)

■ AUTHOR INFORMATION

Corresponding Author

*E-mail: enzo.rotunno@nano.cnr.it.

Author Contributions

The manuscript was written through contributions of all authors. All authors have given approval to the final version of the manuscript.

Notes

The authors declare no competing financial interest.

■ ACKNOWLEDGMENTS

This work is supported by Q-SORT, a project funded by the European Union's Horizon 2020 Research and Innovation Program under grant agreement No. 766970.- Q-SORT (H2020-FETOPEN-1-2016-2017). A.S. and E.K. acknowledge the support of the Ontario Early Researcher Award (ERA) and the Canada Research Chair (CRC) program.

■ REFERENCES

(1) Huang, X.; El-Sayed, I. H.; Qian, W.; El-Sayed, M. A. Cancer cell imaging and photothermal therapy in the Near-Infrared region by using gold nanorods. *J. Am. Chem. Soc.* **2006**, *128*, 2115−2120.

(2) Stiles, P. L.; Dieringer, J. A.; Shah, N. C.; Van Duyne, R. P. Surface-Enhanced Raman Spectroscopy. *Annu. Rev. Anal. Chem.* **2008**, *1*, 601−626.

(3) Atwater, H. A.; Polman, A. Plasmonics for improved photovoltaic devices. *Nat. Mater.* **2010**, *9*, 205−213.

(4) Nelayah, J.; Kociak, M.; Stephan, O.; Garcia de Abajo, F. J.; Tence, M.; Henrard, L.; Taverna, D.; Pastoriza-Santos, I.; Liz-Marzan, L. M.; Colliex, C. Mapping surface plasmons on a single metallic nanoparticle. *Nat. Phys.* **2007**, *3*, 348−353.

(5) Rossouw, D.; Couillard, M.; Vickery, J.; Kumacheva, E.; Botton, G. A. Multipolar Plasmonic Resonances in Silver Nanowire Antennas Imaged with a Subnanometer Electron Probe. *Nano Lett.* **2011**, *11*, 1499−1504.

(6) Schaffer, B.; Hohenester, U.; Trügler, A.; Hofer, F. High-resolution surface plasmon imaging of gold nanoparticles by energy-

DOI: 10.1021/acsphotonics.9b00131
ACS Photonics 2019, 6, 620−627

filtered transmission electron microscopy. *Phys. Rev. B: Condens. Matter Mater. Phys.* **2009**, *79*, 041401.
(7) Boudarham, G.; Kociak, M. Modal decompositions of the local electromagnetic density of states and spatially resolved electron energy loss probability in terms of geometric modes. *Phys. Rev. B: Condens. Matter Mater. Phys.* **2012**, *85*, 24544701−24544705.
(8) Guzzinati, G.; Béché, A.; Lourenço-Martins, H.; Martin, J.; Kociak, M.; Verbeeck, J. Probing the symmetry of the potential of localized surface plasmon resonances with phase-shaped electron beams. *Nat. Commun.* **2017**, *8*, 14999.
(9) Lourenço-Martins, H.; Lubk, A.; Guzzinati, G.; Verbeeck, J.; Kociak, M. *Q-SORT International Conference on Electron Beam Shaping in Space and Time*; Julich, Germany, May 27−30, 2018.
(10) Berkhout, G. C. G.; Lavery, M. P. J.; Courtial, J.; Beijersbergen, M. W.; Padgett, M. J. Efficient Sorting of Orbital Angular Momentum States of Light. *Phys. Rev. Lett.* **2010**, *105*, 153601.
(11) Grillo, V.; Tavabi, A. H.; Venturi, F.; Larocque, H.; Balboni, R.; Gazzadi, G. C.; Frabboni, S.; Lu, P. H.; Mafakheri, E.; Bouchard, F.; Dunin-Borkowski, R. E.; Boyd, R. W.; Lavery, M. P. J.; Padgett, M. J.; Karimi, E. Measuring the orbital angular momentum spectrum of an electron beam. *Nat. Commun.* **2017**, *8*, 15536.
(12) McMorran, B. J.; Harvey, T. R.; Lavery, M. P. Efficient sorting of free electron orbital angular momentum. *New J. Phys.* **2017**, *19*, 023053.
(13) Hossack, W.; Darling, A.; Dahdouh, A. Coordinate Transformations with Multiple Computer-generated Optical Elements. *J. Mod. Opt.* **1987**, *34*, 1235−1250.
(14) Garcia de Abajo, F. J. Optical excitations in electron microscopy. *Rev. Mod. Phys.* **2010**, *82*, 209.
(15) Garcia de Abajo, F. J.; Aizpurua, J. Numerical simulation of electron energy loss near inhomogeneous dielectrics. *Phys. Rev. B: Condens. Matter Mater. Phys.* **1997**, *56*, 15873.
(16) Grillo, V.; Harris, H.; Gazzadi, G. C.; Balboni, R.; Mafakheri, E.; Dennis, M. R.; Frabboni, S.; Boyd, R. W.; Karimi, E. Generation and application of bessel beams in electron microscopy. *Ultramicroscopy* **2016**, *166*, 48−60.
(17) Grillo, V.; Karimi, E.; Gazzadi, G. C.; Frabboni, S.; Dennis, M. R.; Boyd, R. W. Generation of Nondiffracting Electron Bessel Beams. *Phys. Rev. X* **2014**, *4*, 011013.
(18) Ugarte, D.; Ducati, C. Controlling multipolar surface plasmon excitation through the azimuthal phase structure of electron vortex beams. *Phys. Rev. B: Condens. Matter Mater. Phys.* **2016**, *93*, 205418.
(19) Mohammadi, Z.; Van Vlack, C.; Hughes, S.; Bornemann, J.; Gordon, R. Vortex electron energy loss spectroscopy for near-field mapping of magnetic plasmons. *Opt. Express* **2012**, *20*, 15024−15034.
(20) Hohenester, U.; Trügler, A. MNPBEM - A Matlab toolbox for the simulation of plasmonic nanoparticles. *Comput. Phys. Commun.* **2012**, *183*, 370−381.
(21) Kadkhodazadeh, S.; Christensen, T.; Beleggia, M.; Asger Mortensen, N.; Wagner, J. B. The Substrate Effect in Electron Energy-Loss Spectroscopy of Localized Surface Plasmons in Gold and Silver Nanoparticles. *ACS Photonics* **2017**, *4*, 251−261.
(22) Hörl, A.; Haberfehlner, G.; Trügler, G.; Schmidt, F.; Hohenester, U.; Kothleitner, G. Tomographic reconstruction of the photonic environment of plasmonic nanoparticles. *Nat. Commun.* **2017**, *8*, 37.
(23) Unger, G.; Trügler, A.; Hohenester, U. Novel Modal Approximation Scheme for Plasmonic Transmission Problems. *Phys. Rev. Lett.* **2018**, *121*, 246802.
(24) Schmidt, F. P.; Ditlbacher, H.; Hohenester, U.; Hohenau, A.; Hofer, F.; Krenn, J. R. Dark plasmonic breathing modes in silver nanodisks. *Nano Lett.* **2012**, *12*, 5780−5783.
(25) Johnson, P. B.; Christy, R. W. Optical Constants of the Noble Metals. *Phys. Rev. B* **1972**, *6*, 4370.
(26) Schmidt, F. P.; Ditlbacher, H.; Hohenester, U.; Hohenau, A.; Hofer, F.; Krenn, J. R. Universal dispersion of surface plasmons in flat nanostructures. *Nat. Commun.* **2014**, *5*, 3604.
(27) Schmidt, F. P.; Ditlbacher, H.; Hofer, F.; Krenn, J. R.; Hohenester, U. Morphing a Plasmonic Nanodisk into a Nanotriangle. *Nano Lett.* **2014**, *14*, 4810−4815.
(28) Alù, A.; Engheta, N. Dynamical theory of artificial optical magnetism produced by rings of plasmonic nanoparticles. *Phys. Rev. B: Condens. Matter Mater. Phys.* **2008**, *78*, 085112.
(29) Hentschel, M.; Saliba, M.; Vogelgesang, R.; Giessen, H.; Alivisatos, A. P.; Liu, N. Transition from Isolated to Collective Modes in Plasmonic Oligomers. *Nano Lett.* **2010**, *10*, 2721−2726.
(30) Davis, T. J.; Gomez, D. E.; Vernon, K. C. Simple Model for the Hybridization of Surface Plasmon Resonances in Metallic Nanoparticles. *Nano Lett.* **2010**, *10*, 2618−2625.
(31) Cherqui, C.; Wu, Y.; Li, G.; Quillin, S. C.; Busche, J. A.; Thakkar, N.; West, C. A.; Montoni, N. P.; Rack, P. D.; Camden, J. P.; Masiello, D. J. STEM/EELS Imaging of Magnetic Hybridization in Symmetric and Symmetry-Broken Plasmon Oligomer Dimers and All-Magnetic Fano Interference. *Nano Lett.* **2016**, *16*, 6668−6676.
(32) Asenjo-Garcia, A.; García de Abajo, F. J. Dichroism in the Interaction between Vortex Electron Beams, Plasmons, and Molecules. *Phys. Rev. Lett.* **2014**, *113*, 066102.
(33) Harvey, T. R.; Pierce, J. S.; Chess, J. J.; McMorran, B. J. Demonstration of electron helical dichroism as a local probe of chirality. *ArXiv:1507.01810*, **2015**.
(34) Larocque, H.; Bouchard, F.; Grillo, V.; Sit, A.; Frabboni, S.; Dunin-Borkowski, R. E.; Padgett, M. J.; Boyd, R. W.; Karimi, E. Nondestructive Measurement of Orbital Angular Momentum for an Electron Beam Phys. *Phys. Rev. Lett.* **2016**, *117*, 154801.
(35) Vanacore, G. M.; Berruto, G.; Madan, I.; Pomarico, E.; Biagioni, P.; Lamb, R. J.; McGrouther, D.; Reinhardt, O.; Kaminer, I.; Barwick, B.; Larocque, H.; Grillo, V.; Karimi, E.; García de Abajo, F. J.; Carbone, F.Ultrafast generation and control of an electron vortex beam via chiral plasmonic near fields. *ArXiv:1806.00366*, **2018**.

DOI: 10.1021/acsphotonics.9b00131
ACS Photonics 2019, 6, 620−627